THE ASTROPHYSICAL JOURNAL, 402:3–14, 1993 January 1

$H_0 = 43 \pm 11$ km s^{-1} Mpc^{-1} BASED ON ANGULAR DIAMETERS OF HIGH-LUMINOSITY FIELD SPIRAL GALAXIES

ALLAN SANDAGE
The Observatories of the Carnegie Institution of Washington, 813 Santa Barbara Street, Pasadena, CA 91101
Received 1992 January 10; accepted 1992 June 30

ABSTRACT

Eight methods that favor the long extragalactic distance scale with H_0 near 50 km s^{-1} Mpc^{-1} are contrasted with two methods that require the short distance scale with H_0 near 85 km s^{-1} Mpc^{-1}. A ninth method is developed in this paper that requires the long scale, based on relative linear diameters of luminous field spirals compared with the known linear diameter of M101.

Eighty-six field galaxies with a similar morphology to M101 have been identified in the Revised Shapley-Ames Catalog. The linear diameter distribution of this sample shows the expected Malmquist bias as a function of redshift because the galaxies are selected from the flux-limited rather than a distance-limited catalog.

The mean relative linear diameter of the sample, based on an arbitrary Hubble constant and corrected for Malmquist bias, is compared with the linear diameter of M101, known from its Cepheid distance. If the mean diameter of the unbiased field galaxy sample is the same as the linear diameter of M101, then

$$H = 43 \pm 11 \text{ km s}^{-1} \text{ Mpc}^{-1} .$$

The correction of this local value ($\langle v_0 \rangle = 3000$ km s^{-1}) to the global cosmological Machian expansion frame is small, giving H_0 (global) < 50 km s^{-1} Mpc^{-1} by this method.

If H_0 were in fact as high as 85, either (1) our adopted distance to M101 is too large by a factor of 2 or (2) M101 must be among the largest several Sc I galaxies within a distance of $\sim$4000 km s^{-1}. The first is impossible because of the known Cepheid distance. The second is unlikely because similar analysis of angular diameter data for field galaxies similar to M31 give the same result, showing either that M101 is not abnormal or that M101 and M31 are both equally abnormal, being among the largest galaxies of their class within the available distance-limited sample.

Subject headings: cosmology: observations — distance scale — galaxies: fundamental parameters — galaxies: spiral

1. INTRODUCTION

There is a perception abroad that "a large value of the Hubble parameter $H_0 \sim 75$ km s^{-1} Mpc^{-1} ... seems increasingly favored by the observations" (Lahav et al. 1991). It has also been said that "none of [the four methods that give $H_0 \sim 50$] is empirically reliable" (Fukugita & Hogan 1991, hereafter FH; see also Fukugita & Hogan 1990). If in fact $H_0 \sim 75$, it becomes necessary to introduce the cosmological constant if the long time scale from the age of the chemical elements, the age of the globular cluster system, and the age of the Galaxy are to be reconciled with the expansion.

The purpose of this paper is to argue (1) that the available evidence does not establish the short distance scale and that the conclusion to that effect by FH is premature; (2) that various methods to H_0 are contradictory; to advocate the short distance scale requires neglect of eight methods, plus the method developed here, that favor the long scale; to advocate the long distance scale requires neglect of only two methods, and these are not yet fully understood; and (3) that the most likely range of H_0 from the method developed here is $32 < H_0 < 54$ km s^{-1} Mpc^{-1}, giving the range of the inverse Hubble constant as $30 > H_0^{-1} > 18$ Gyr.

Although we do not debate the FH position, it is useful to balance the prolusion with which FH neglect the long distance scale. The methods and counterarguments showing that this scale cannot be dismissed in their way are as follows.

FH decide that the distance modulus of Virgo is $(m - M)_0 = 30.9$. Their resulting distance of $D = 15$ Mpc leads to a high value of $H_0 = 76$ km s^{-1} Mpc^{-1} when combined with the Virgo Cluster redshift reduced to the proper Machian frame (Sandage & Tammann 1990, hereafter ST90). In their analysis, FH rely mainly on the methods based on planetary nebulae (PNs) (Jacoby 1989; Jacoby et al. 1989; Jacoby, Ciardullo, & Ford 1990) and on surface brightness (SB) fluctuations (Tonry & Schneider 1988; Tonry, Ajhar, & Luppino 1989).

FH adopt their short distance scale using PN and SB precepts that contain unsolved problems.

1. As presently applied, Bottinelli et al. (1991) show that apparent PN distances for galaxies known to be at the same distance depend on the absolute magnitude of the parent galaxy; there is a richness effect. Therefore, the PN luminosity function is not infinitely sharp at the bright end as required by Jacoby and collaborators. Although the effect is small, its existence shows that the current use of the PN method cannot be entirely correct; apparently more must be understood about PN evolution. The serious contradiction between the PN method and the results from the eight methods set out below that require the long distance scale show that hidden systematic problems yet remain in the PN method unless all the methods that lead to the long scale are themselves wrong.

2. Tammann (1992) shows that distances using the SB method, again for galaxies at the same distance, vary with the metal abundance; the calibration of the SB method depends on the nature of the dominant galaxian stellar population, a variation presently unaccounted for.

Nevertheless, the impressive internal tests now in the liter-

ature for these two methods present the most severe challenge to the long distance scale. For this reason FH believe that the PN and SB results are overridingly powerful. But the adumbration of FH that "none of the [long distance scale] methods are empirically reliable" is obdurate.

1. FH neglect two analyses of the Tully-Fisher (TF) method in which complete galaxy samples in the Virgo Cluster are used (Kraan-Korteweg, Cameron, & Tammann 1988, hereafter KKCT; Fouqué et al. 1990, hereafter FBGP). KKCT show that the TF method applied to the (nearly) complete sample gives $D_{\rm Virgo} = 21$ Mpc leading to $H_0 = 50$. On the other hand, Pierce & Tully (1988) obtained $(m - M)_0 = 31.0$, $D = 16$ Mpc from their analysis of an incomplete sample. Both KKCT and FBGP show that incomplete samples lead to too small a distance by about 30% caused by bias problems.

FBGP have also obtained the large Virgo distance modulus of $(m - M)_0 = 31.6$ by analyzing a nearly complete sample of Virgo Cluster galaxies via the TF method using the KKCT system of calibrators. This modulus requires $H_0 = 55$, adopting the cosmological velocity of Virgo as v(cosmic) = 1144 km s^{-1} (ST90).

FH also neglect the evidence that systematic bias problems exist in the TF analysis of the field galaxies in the catalog of Aaronson et al. (1982). The Malmquist bias is eliminated by restricting this sample to the distance-limited subset of galaxies with $v < 500$ km s^{-1}. Used with the local calibrators, this subset gives $H_0 \sim 50$ (Sandage 1988b, Fig. 9, hereafter S88b). The point is important because the total Aaronson et al. sample contains a strong Malmquist bias. The evidence is that the apparent value of H increases with redshift when the total sample is used (the S88a, Fig. 9 argument applied to the S88b analysis). But this putative increase of H with redshift is an artifact of the total biased data (Sandage 1988a, b). Adding a fainter sample revealed that H would be calculated to be double-valued at a given distance when the data are analyzed by neglecting the bias—an obvious contradiction.

Huchtmeier & Richter (1986) also obtain $H = 50$ with the TF method in an independent analysis of the Kraan-Korteweg & Tammann (1979) 500 km s^{-1} distance-limited sample (see also S88b, Fig. 9); here the Malmquist bias is clearly absent, making this result particularly well determined.

2. Tammann (1988), in a critique of the D_n-σ method (Dressler et al. 1987), shows that use of data that are corrected for selection effects gives $(m - M)_0 = 31.85$ for the Virgo modulus, not $(m - M)_0 = 30.9$ quoted by FH. This leads to $H_0 = 48$ compared with $H_0 = 76$ suggested by FH from the same data.

3. The argument through Type Ia supernovae shows that the absolute magnitude of SN Ia of $M_{B(\rm max)} = -18.5$ derived by FH is 1.3 mag fainter than the most successful theoretical models of the SN Ia deflagration. The latest version by Hoflich, Khokhlov, & Muller (1991), following earlier work by authors summarized elsewhere (ST90), reproduces the shape of the standard SN Ia light curve, but only if the theoretical calibration is adopted to be $M_B(\rm max) = -19.8$. This calibration is identical with the observational calibration by Leibundgut & Tammann (1990) and from independent data based on the distance to IC 4182 (Sandage & Tammann 1982), recently confirmed from Cepheids found with *HST* in IC 4182 (Sandage et al. 1992). These calibrations, plus the available photometric data on SN Ia's in field galaxies with appreciable redshifts, give a Hubble constant of $H_0 = 46 \pm 10$ km s^{-1} Mpc^{-1} (Tammann & Leibundgut 1990).

4. The resolution of the radio disk of the Type II supernova 1979c in M100 gives $(m - M)_0 = 31.70$ as modeled by Bartel (1989). Branch et al. (1981) obtained an expansion parallax modulus of $(m - M)_0 = 31.80$ for the same SN, leading $D = 22.9$ Mpc and therefore $H_0 = 50$.

5. The globular cluster luminosity function for Virgo Cluster E galaxies (Harris 1988) gives $(m - M)_0 = 31.74$ (ST90, § 6.1) leading to $H_0 = 51$ (Tammann 1992).

6. Normal novae in Virgo E galaxies (Pritchet & van den Bergh 1987) give $(m - M)_{\rm (Virgo)} = 31.57$ following the discussion by Sandage & Tammann (1988, 1990).

Two modern methods based on new physics, often anticipated but now with first results, support the long distance scale.

7. Birkinshaw, Hughes, & Arnauld (1991) find $H_0 = 37 \pm 9$ km s^{-1} Mpc^{-1} from the observed Sunyaev-Zeldovich effect on the Comptonization of the 3° radiation by the X-ray gas in the cluster of galaxies Abell 665.

8. Press, Rybicki, & Hewitt (1992) also find $H_0 = 37$ km s^{-1} Mpc^{-1} using the time delay of luminosity bursts in the images of the gravitational lens 0957+561, following earlier work by Rhee (1991) who obtained $H_0 \sim 50$ by the same method using a less certain time delay.

Clearly, the problem of the Hubble constant has not been solved in favor of either scale. The absence of an experiment so clean and compelling that it negates all others keeps the problem open. But as an interim exercise we set out in the present paper details of a method used by van der Kruit (1986), suggested earlier by Baade (Humason, Mayall, & Sandage 1956, Appendix C), based on angular diameters of local galaxies. As applied here, luminous Sc galaxies similar to M101 comprise the sample. Distances from redshifts convert angular diameters to relative linear diameters. Calibration with M101 changes the relative scale to absolute and leads to the local value of H. Tie-in of the local velocity frame to the cosmic Machian frame by standard methods (ST90) yields the global value of H_0.

2. JUSTIFICATION OF USE OF ISOPHOTAL ANGULAR GALAXY DIAMETERS

2.1. *Relation between Exponential Scale Lengths and Isophotal Diameters*

An objection to the use of isophotal diameters as standard rods is that diameters defined to an assigned surface brightness will vary for galaxies with different average surface brightnesses which otherwise have identical e-folding exponential scale lengths. Galaxies with small average surface brightness will have small isophotal diameters for given disk exponential scale lengths. On the other hand, isophotal diameters and exponential scale lengths will differ by only a well-defined fixed factor if the central surface brightness of galaxy disks is nearly constant from galaxy to galaxy. Isophotal diameters would then provide a good measure of metric disk scale lengths.

This ideal situation would be realized if Freeman's (1970) result is true that the central surface brightness of the disks of luminous spirals is nearly constant. Kormendy (1977), and more particularly Disney (1976), doubted Freeman's result, suggesting that the apparent constancy of $I(0)$ in Freeman's sample is a selection effect. These objections now seem unlikely based on the rediscussions by Freemann (1978, 1979) and on a new study by van der Kruit (1987) which confirms Freemann's conclusion.

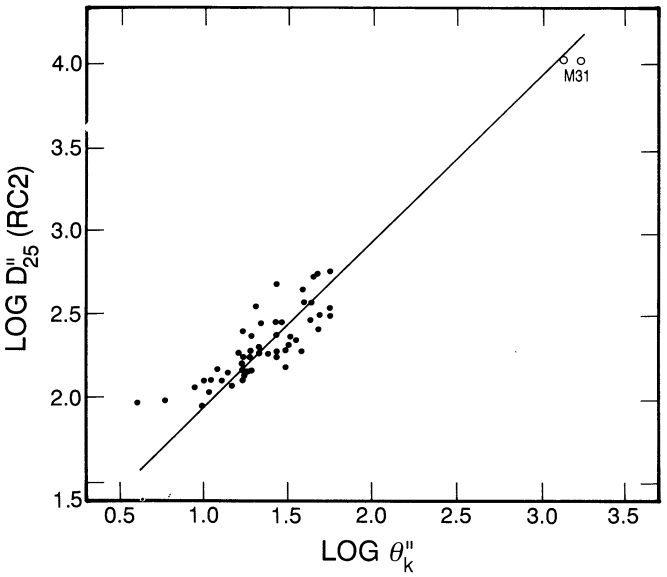

FIG. 1.—(*Filled circles*): Comparison of the RC2 D_{25} angular diameters (in arcsec) with the exponential scale lengths measured by Kent (1985) for a variety of galaxy types. *Open circles*: Same for M31 adopting the linear disk exponential scale lengths given by Freeman (1970) and by van der Kruit (1987), changed to angular measure using $(m - M)_0 = 24.2$ for M31.

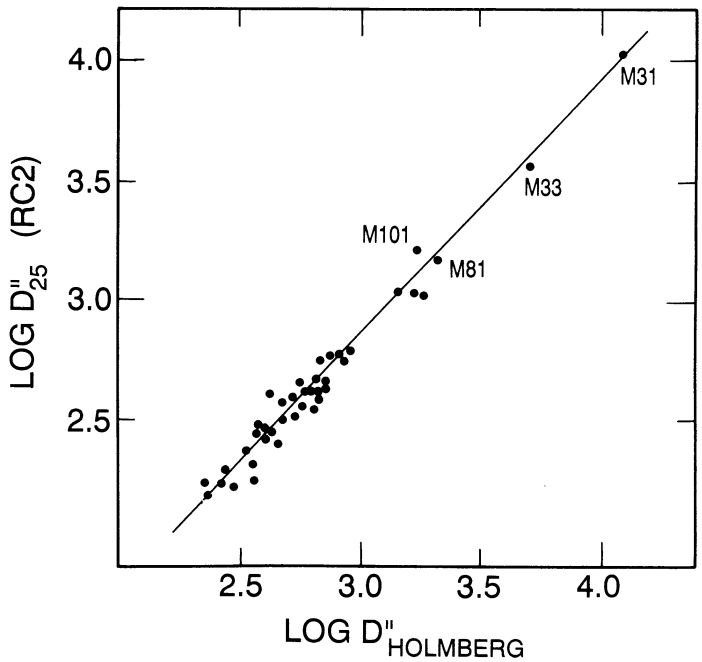

FIG. 2.—Comparison of RC2 D_{25} angular diameters with $D_{26.5}$ diameters measured by Holmberg (1950, 1958) for a representative subset of galaxies in common.

We can also demonstrate the proposition by showing the tight relation between the D_{25} isophotal angular diameters listed in the RC2 (de Vaucouleurs, de Vaucouleurs, & Corwin 1976) and the exponential scale lengths determined by Boroson (1981), Boroson, Strom, & Strom (1983), Kent (1985), and van der Kruit (1987).

Figure 1 shows the correlation. The scale lengths are measured by Kent (1985); the isophotal diameters are from the RC2. The two abscissa values for M31 are the estimated linear exponential scale lengths of 4.5 kpc from Freeman (1970) and 5.5 kpc from van der Kruit (1987), changed to angular scale lengths of 1349″ and 1660″ using a distance modulus of $(m - M)_0 = 24.2$. The M31 isophotal angular diameter from the RC2 is 1.1×10^4 arcsec.

The ratio of RC2 isophotal diameters to exponential scale lengths is $D_{25}/\theta_{\rm Kent} = 8.9$, based on the logarithmic zero-point offset of 0.95 between ordinate and abscissa in Figure 1. Similar correlations exist with the data of van der Kruit (1987), and of Boroson (1981), and Boroson et al. (1983). The logarithmic zero-point offsets in the equivalent of Figure 1 in these two independent studies are 0.90 for the van der Kruit data, and between 0.72 and 0.80 in the two studies of Boroson and Boroson et al. Knapen & van der Kruit (1991) give a summary of the differences in the systems of measured scale lengths by various authors. For our purposes the only important point from Figure 1 is that scale lengths and D_{25} diameters are well correlated.

2.2. *Reliability of the RC2 Isophotal Diameters*

The reliability of the RC2 isophotal diameters is tested in Figure 2 where RC2 diameters are plotted versus isophotal diameters measured by Holmberg (1950, 1958). Holmberg's photometry is based on out-of-focus images of standard stars in the North Polar Sequence and in SA 57, compared with in-focus images of the galaxies. The galaxy images were microphotometered and integrated over the area, providing the most precise body of total magnitudes and isophotal diameters in the literature for individual large nearby galaxies before the advent of large-format CCD detectors.[1]

Our conclusions from Figures 1 and 2 are (1) RC2 diameters are reliable measurements of isophotal diameters (Fig. 2) and (2) the listed RC2 isophotal diameters are good measures of metric scale lengths for luminous Sc galaxies (Fig. 1). We have, then, a measure of a "standard metric rod" which, when calibrated, can be used to determine a system of geometrical distances, and therefore the Hubble constant. This demonstration, of course, says nothing about the efficacy of such metric rods as distance indicators. We show later (§ 5.3) that the dispersion is $\sigma(\log D) \sim 0.10$ (or $\sigma M \sim 0.5$ mag) which is larger by at least a factor of 2 than for SN Ia (Sandage et al. 1993) but is smaller than for spiral galaxies of all types and luminosity classes.

3. ANGULAR AND LINEAR DIAMETER DATA FOR Sc GALAXIES

3.1. *Angular Diameters of M101-like Galaxies in the Virgo Cluster*

The four giant spirals in the Virgo Cluster Catalog (Binggeli, Sandage, & Tammann 1985) that most closely resemble the morphology of M101 are listed in Table 1, shown in the Atlas of Virgo Cluster Spirals (Sandage, Binggeli, & Tammann 1985)

[1] Holmberg's listed diameters refer to the well-calibrated isophotal level of $m_{pg} = 26.5$ mag arcsec^{-2} (or 26.6 B mag arcsec^{-2}). The RC2 diameter system refers to a brighter isophote. The zero-point offset of the line of unit slope in Fig. 2 is $\log D_{\rm Holmberg}/D_{\rm RC2} = 0.14$, or $D_{\rm Holmberg}/D_{\rm RC2} = 1.38$. If the ratio of RC2 *radii* to exponential scale length is taken to be 3.8 based on the average of the determinations by Kent ($0.5D_{25}/{\rm SL} = 4.5$), van der Kruit (4.0), and Boroson (2.9), the Holmberg radius is larger than the RC2 radius by 1.46 scale lengths, corresponding to a magnitude difference of 1.59 mag. Holmberg states that his diameters refer to an isophote at 26.6 B arcsec^{-2}. Therefore, the RC2 isophote level is 26.6 − 1.59 = 25.0 B arcsec^{-2}, precisely the value listed in the RC2.

TABLE 1

THE FOUR LARGEST VIRGO CLUSTER Sc I SPIRALS COMPARED WITH M101

NAME (1)	TYPE (2)	HOLMBERG D_{MA} (3)	HOLMBERG a/b (4)	$D(0)_{25}$ RC2 (5)	$D(0)_{25}$ RC3 (6)
NGC 4254	Sc(s) I.3	7.3	1.22	5.2	5.6
NGC 4303	Sc(s) I.2	10.7	1.44	5.9	6.5
NGC 4321	Sc(s) I	10.0	1.10	6.8	7.6
NGC 4535	SBc(s) I.3	9.9	1.11	6.3	7.6
M101	Sc(s) I	28.0	1.0	26.9	28.8

printed to the same scale. A fifth spiral with slightly later morphology is NGC 4654 [SBc(rs) II] with a Holmberg major diameter of 7.0 and a listed RC2 major diameter of 4.3.

Column (2) of Table 1 shows the morphological type listed in the RSA2 (Sandage & Tammann 1987). Holmberg's (1958) major axis angular diameter and the axial ratio are listed in columns (3) and (4). The listed D_{25} angular diameters from the RC2 and RC3 are in columns (5) and (6).

Use of the Virgo Cluster Sc I angular diameters as a distance indicator, taken in ratio to M101, was argued earlier (Sandage & Tammann 1976, Fig. 6). Adopting a distance to M101 (§ 4.1), we shall use the argument again in § 4.2 to obtain the distance to the Virgo Cluster using the data in Table 1.

However, it is not clear that the distance to the Virgo Cluster core can be obtained by study of the spirals that generally inhabit the outer cluster regions and that have a high velocity dispersion. The velocity properties of spirals just arriving in the vicinity of the cluster by infall (Tully & Shaya 1984; Sandage 1990; Teerikorpi et al. 1992) have been analyzed to show large distance differences between spirals and the cluster core. Any Virgo distance based only on individual spirals, said in some catalogs to be cluster members, may be unreliable due to this infall problem (Teerikorpi et al. 1992). In the present paper we have circumvented this direct method based on Virgo Cluster spirals (but after first applying it in the next section) by carrying the diameter comparison into the general field, using the complete all-sky sample of spirals in the Revised Shapley-Ames Catalog (RSA2) that have the M101 morphology. This bypasses all questions of possible unsuitability of Virgo Cluster spirals, making moot the conclusions of Pierce, McClure, & Racine (1992) and of Shanks et al. (1992) concerning the distance to the Virgo Cluster core found from the resolution of Virgo spirals into individual stars as if the spiral distance defines the distance to the elliptical rich core.

3.2. *Data for the Angular Diameters of Field Sc I Galaxies*

To obtain a sample of field M101 look-alike galaxies, we reinspected the large-scale survey plates used for the RSA2 morphological classifications for the Carnegie Atlas of Bright Galaxies (Sandage & Bedke 1993). Eighty-six non–Virgo Cluster galaxies were identified whose morphological types are similar to M101.

The data are set out in Tables 2–4. The morphological type in column (2) is from the RSA2. The redshift, corrected to the centroid of the Local Group and then to the Virgo Cluster frame for an infall velocity of the Local Group of 220 km s^{-1}, is in column (3). The data sources are the RSA2 and the catalog of the Virgocentric flow model by Kraan-Koretweg (1986) following the original model of Silk (1974, 1977), as developed further by Schechter (1980), and Tonry & Davis (1981). We have adopted $v_{infall} = 220$ km s^{-1} determined by Tammann & Sandage (1985). Experimentation with different infall velocities from 0 to 440 km s^{-1} shows negligible differences to the conclusions here.

Column (5) contains the log of the angular diameter from the RC2 (unit is 0.1). Column (6) is the log of the linear diameter (in parsecs) based on a linear redshift-distance relation and a Hubble constant of 50 km s^{-1} Mpc^{-1}. Column (7) lists the absolute B magnitudes from the RSA2 corrected for Galactic absorption and for inclination, again based of $H = 50$.

4. THE HUBBLE CONSTANT FROM THE VIRGO CLUSTER SPIRALS ALONE

4.1. *Adopted Distance and Linear Diameter of M101*

The adopted distance to M101 is $(m - M)_0 = 29.3$ (Sandage & Tammann 1974b), for a distance of $D = 7.24$ Mpc, to which we put an error of $\pm 8\%$ based on an assumed error of ± 0.2 mag in the distance modulus. This distance is more than 10 times Hubble's (1926, 1936; Hubble & Humason 1931) and has been confirmed by Cook, Aaronson, & Illingworth (1986) by their discovery of Cepheids.

The isophotal diameter of M101 is adopted as $D_{25} = 26.9$, based (mostly) on the precise measurement by Holmberg, reduced to the isophotal level of the RC2 as listed there. The known accuracy of the Holmberg diameters is at the level of $\pm 5\%$ (Holmberg 1950, 1958; and the discussion in the RC2).

The linear isophotal diameter of M101 is 56.6 kpc based on these adopted distance and angular diameter data. The error is put at $\pm 9\%$, or $\log D_{25} = 4.75 \pm 0.04$.

4.2. *The M101 Calibration Applied to the Virgo Cluster Spirals*

Consider first the mean of the angular diameters of the four Sc I galaxies in Table 1 as if this mean corresponds to the size of M101 itself. The mean of the column (5) entries in Table 1 is $\langle D_{25} \rangle = 6.05$, giving the diameter ratio to M101 as $D_{25}(\mathrm{M101})/\langle D_{25\,\mathrm{Virgo}} \rangle = 4.45$. If the RC3 values in column (6) are used instead, the diameter ratio is nearly the same at 4.22. Using the mean ratio as 4.33 and the M101 distance of 7.24 Mpc gives the distance to Virgo as 31.3 Mpc on the assumption that the spirals are, in fact, at the mean distance of the E galaxies in the Virgo core.

If we restrict the comparison to NGC 4321, which is the largest Virgo cluster spiral, the distance ratios are 3.96 from column (5) and 3.79 from column (6), giving Virgo distances of 28 Mpc and 27.4 Mpc. The Hubble constant from this mean Virgo distance of 27.7 Mpc would be

$$H_0 = 41 \pm 4 \text{ km s}^{-1} \text{ Mpc}^{-1}, \quad (1)$$

from equation (27) of ST90 which is $H_0 = 52(21.9/D_{\mathrm{Mpc}})$. The assigned error in equation (1) is based on the assumed 9% error in the M101 data and an assumed 5% error in the angular diameter of NGC 4321.

It is important to note that if we were to adopt the distance to Virgo to be 15 Mpc on the short distance scale, then M101 must have twice the linear diameter of the largest spiral in Virgo (Table 1). This is the same conclusion reached by van der Kruit (1986) using independent angular diameter data on exponential scale lengths directly.

TABLE 2

REDSHIFTS, DIAMETERS, AND MAGNITUDES FOR Sc I–I.3 AND SBc I–I.3 GALAXIES THAT ARE SIMILAR TO M101

Name (1)	Type (2)	v_0^{220} (km s^{-1}) (RSA2 + RKK) (3)	log v_0^{220} (4)	log $\theta(0)$ (0.1) (RC2) (5)	log D(pc) +log (H/50) (6)	$-M_{BT}^{0,i}$ (RSA2) (7)
NGC 309	Sc(r) I	5606	3.749	1.48	4.99	23.17
NGC 628	Sc(s) I	819	2.913	2.01	4.69	21.64
NGC 958	Sc(s) I.2	5700	3.756	1.34	4.86	22.97
NGC 1232	Sc(rs) I	1712	3.233	1.88	4.88	22.49
NGC 1376	Sc(s) I	4102	3.613	1.30	4.68	22.14
NGC 2207	Sc(s) I.2	2653	3.424	1.59	4.78	23.02
NGC 2280	Sc(s) I.2	1812	3.258	1.70	4.73	21.75
NGC 2776	Sc(rs) I	2920	3.465	1.45	4.68	21.99
NGC 2942	Sc(s) I.3	4635	3.666	1.33	4.76	22.44
NGC 2955	Sc(s) I	7252	3.860	1.19	4.82	22.90
NGC 2989	Sc(s) I	4138	3.617	1.12	4.50	21.72
NGC 2997	Sc(s) I.3	995	2.998	1.89	4.66	21.87
NGC 2998	Sc(rs) I	5034	3.702	1.41	4.88	22.93
NGC 3294	Sc(s) I.3	1922	3.284	1.46	4.51	21.23
NGC 3464	Sc(rs) I	3834	3.584	1.42	4.77	22.11
NGC 3478	Sc(s) I	6947	3.842	1.38	4.99	23.33
NGC 3614	Sc(r) I	2683	3.429	1.61	4.81	21.90
NGC 3893	Sc(s) I.2	1331	3.124	1.59	4.48	21.48
NGC 3938	Sc(s) I	1058	3.025	1.73	4.52	21.03
IC 764	Sc(s) I.2	2171	3.337	1.59	4.69	21.95
NGC 4254	Sc(s) I.3	1144V	3.058V	1.72	4.55	21.76
NGC 4303	Sc(s) I.2	1144V	3.058V	1.77	4.59	22.01
NGC 4321	Sc I	1144V	3.058V	1.83	4.66	22.08
NGC 4535	SBc(s) I.3	1144V	3.058V	1.80	4.62	22.15
NGC 4653	Sc(rs) I.3	2817	3.450	1.40	4.62	21.24
NGC 5161	Sc(s) I	2403	3.381	1.64	4.79	22.17
NGC 5364	Sc(r) I	1565	3.194	1.81	4.77	21.84
NGC 5457	Sc(s) I	394	2.595	2.43	4.75[a]	20.91
NGC 5660	Sc(s) I.2	2729	3.436	1.44	4.64	21.69
NGC 6878	Sc(r) I.3	5734	3.758	1.19	4.72	21.71
A2120-46	Sc(s) I	2552	3.407	1.51	4.68	21.76

[a] Based on Cepheid distance.

TABLE 3

REDSHIFTS, DIAMETERS, AND MAGNITUDES FOR Sbc I–I.3 AND SBbc I–I.3 GALAXIES THAT ARE SIMILAR TO M101

Name (1)	Type (2)	v_0^{220} (km s^{-1}) (RSA2 + RKK) (3)	log v_0^{220} (4)	log $\theta(0)$ (0.1) (RC2) (5)	log D(pc) +log (H/50) (6)	$-M_{BT}^{0,i}$ (RSA2) (7)
NGC 1241	SBbc(rs) I.2	3957	3.597	1.44	4.80	22.51
NGC 1365	SBbc(s) I	1454	3.163	1.93	4.86	22.87
NGC 1566	Sbc(s) I.2	1321	3.121	1.86	4.75	22.32
NGC 2223	SBbc(r) I.3	2601	3.415	1.51	4.69	22.10
NGC 2336	SBbc(r) I	2589	3.413	1.78	4.96	23.09
NGC 2713	Sbc(s) I	3916	3.593	1.51	4.87	22.60
NGC 3054	SBbc(s) I	2191	3.341	1.55	4.66	21.97
NGC 3124	SBbc(r) I	3561	3.552	1.49	4.81	22.39
NGC 3145	SBbc(rs) I	3681	3.566	1.45	4.78	22.60
NGC 3259	Sbc(r) I	2261	3.354	1.31	4.43	21.16
NGC 3344	Sbc(rs) I.2	646	2.810	1.83	4.41	20.42
NGC 3433	Sbc(r) I.3	2919	3.465	1.54	4.77	21.86
NGC 3486	Sbc(r) I.2	646	2.810	1.81	4.39	20.09
NGC 3687	SBbc(r) I.2	2818	3.450	1.31	4.53	21.31
NGC 3720	Sbc(s) I	6095	3.785	1.02	4.57	22.03
NGC 3963	Sbc(r) I.2	3549	3.550	1.44	4.76	22.18
NGC 4030	Sbc(r) I	1796	3.254	1.60	4.62	22.09
NGC 4939	Sbc(rs) I	3235	3.510	1.70	4.98	23.00
NGC 5324	Sbc(r) I.3	3183	3.503	1.38	4.65	21.88
NGC 5351	Sbc(rs) I.2	3954	3.597	1.43	4.79	22.24
NGC 5426	Sbc(rs) I.2	2798	3.447	1.40	4.61	21.46
NGC 5427	Sbc(s) I	2900	3.462	1.39	4.62	22.05
NGC 5905	SBbc(rs) I	3769	3.576	1.59	4.93	22.61
NGC 6699	Sbc(s) I.2	3383	3.529	1.27	4.57	21.93

TABLE 4

REDSHIFTS, DIAMETERS, AND MAGNITUDES FOR Sbc I-II AND SBbc I-II GALAXIES THAT ARE SIMILAR TO M101

Name (1)	Type (2)	v_0^{220} (km s^{-1}) (RSA2 + RKK) (3)	log v_0^{220} (4)	log $\theta(0)$ (0.1) (RC2) (5)	log D(pc) +log (H/50) (6)	$-M_{BT}^{0,i}$ (RSA2) (7)
NGC 214	Sbc(r) I–II	4636	3.666	1.30	4.73	22.35
NGC 289	SBbc(rs) I–II	1734	3.239	1.54	4.55	21.51
IC 1788	Sbc(s) I–II	3250	3.512	1.31	4.59	21.53
NGC 976	Sbc(r) I–II	4451	3.648	1.21	4.62	21.85
NGC 1625	Sbc(s) I–II	3009	3.478	1.30	4.55	21.57
NGC 1640	SBbc(r) I–II	1606	3.206	1.41	4.38	20.57
NGC 2347	Sbc(r) I–II	4818	3.683	1.28	4.73	22.38
NGC 3001	SBbc(s) I–II	2412	3.382	1.45	4.60	21.42
NGC 3162	Sbc(s) I.8	1582	3.199	1.48	4.45	20.68
NGC 3338	Sbc(s) I–II	1569	3.196	1.70	4.66	21.59
NGC 3430	Sbc(rs) I–II	1938	3.287	1.54	4.59	21.26
NGC 3506	Sbc(s) I–II	6605	3.820	1.12	4.71	22.63
NGC 3953	SBbc(r) I–II	1331	3.124	1.76	4.65	21.84
NGC 4045	Sbc(s) I–II	2207	3.344	1.41	4.52	20.96
NGC 4123	SBbc(rs) I.8	1676	3.224	1.62	4.61	21.15
NGC 4536	Sbc(s) I–II	1144V	3.058V	1.79	4.61	21.26V
NGC 4603	Sbc(s) I–II	2340	3.369	1.54	4.68	21.92
NGC 4891	SBbc(r) I–II	2769	3.442	1.43	4.64	21.65
NGC 4947	Sbc(s) I–IIpec	2503	3.398	1.40	4.57	21.39
NGC 5194	Sbc(s) I–II	593	2.773	2.00	4.54	21.80
NGC 5248	Sbc(s) I–II	1517	3.181	1.78	4.73	21.99
NGC 5350	SBbc(rs) I–II	2642	3.422	1.49	4.68	21.77
NGC 5430	SBbc(s) I.8	3267	3.514	1.33	4.61	21.97
NGC 5592	Sbc(s) I–II	4415	3.645	1.19	4.60	21.99
NGC 5921	SBbc(s) I–II	1751	3.243	1.67	4.68	21.58
NGC 6780	Sbc(rs) I–II	3389	3.530	1.26	4.56	21.51
NGC 6814	Sbc(rs) I–II	1686	3.227	1.50	4.49	21.27
NGC 6925	Sbc(r) I–II	2745	3.438	1.51	4.72	22.33
NGC 6984	Sbc(r) I.8	4375	3.641	1.20	4.61	21.87
NGC 7038	Sbc(s) I.8	4705	3.673	1.43	4.87	23.02
NGC 7124	Sbc(rs) I–II	4870	3.687	1.35	4.80	22.46
NGC 7171	Sbc(r) I–II	2663	3.425	1.39	4.58	21.38
NGC 7392	Sbc(s) I–II	2911	3.464	1.26	4.49	21.63
NGC 7479	SBbc(s) I–II	2532	3.403	1.59	4.76	22.25
NGC 7531	Sbc(r) I–II	1545	3.189	1.45	4.40	21.23
NGC 7755	SBbc(r)/Sbc(r) I–II	2850	3.455	1.55	4.77	22.05

5. THE METHOD OF ANGULAR DIAMETERS APPLIED TO FIELD Sc I GALAXIES

5.1. *Correlation of Linear Diameters with Redshift*

As discussed earlier, large spirals projected near the Virgo Cluster core may not be at the distance of the core (Teerikorpi et al. 1992). In addition, there may be environmental effects for galaxies in the harsh environment of the Virgo Cluster. Consequently we circumvent objections to the results of § 4 by applying the method to the field spirals in Tables 2–4.

The full Malmquist bias exists for this sample because the galaxies are taken from a flux-limited catalog rather than being distance-limited. The bias problem is the same as was discussed using magnitudes for a similar sample of Shapley-Ames galaxies (Sandage 1988a, hereafter S88a). The solution to remove the bias is also similar to the discussion there.

The linear diameters in parsecs listed in columns (6) of Tables 2–4, based on RC2 angular diameters, are calculated from the v^{220} redshifts using $H_0 = 50$. The log of these diameters are plotted in Figure 3*a* versus the log v^{220} from column (4). Crosses are for the Sc I–I.3 galaxies in Table 2, filled circles are the Sbc I–I.3 galaxies in Table 3, and triangles are the Sbc I–II galaxies in Table 4 to which 0.03 has been added to the log D_{25} values to correct for the systematic smaller angular diameters of Sbc I–II galaxies compared with Sbc I–I.3 and Sc I–I.3 galaxies at a given redshift (see S88a for the justification). This correction has been determined by comparing the three diagrams of angular diameters versus log v^{220} from the data in Tables 2–4 for the various types.

The systematic increase of log D(pc) with redshift in Figure 3*a* is evident. The mean values change from $\langle \log D(\mathrm{pc}) \rangle = 4.68$ at $\langle \log v^{220} \rangle = 3.2$ to $\langle \log D(\mathrm{pc}) \rangle = 4.83$ at $\langle \log v^{220} \rangle = 3.8$. This effect is the most direct signature of the Malmquist bias (Sandage 1972, Fig. 7; Sandage, Tammann, & Yahil 1979; S88a, b). It is not due to the Hubble constant increasing outward (Tully 1988) nor to a nonlinear redshift-distance relation everywhere (Segal 1982) as was proved elsewhere (S88a) by adding a fainter sample and analyzing the consequences.

Following S88a, b, the upper and lower envelope lines expected for a distance-limited sample are shown in Figure 3*b*, calculated using a Gaussian distribution of linear diameters with the condition that the lines represent the locus of one galaxy in the upper and lower wings of the distribution. The opening of these lines with increasing redshift is due to the increased volume between redshifts v and $v + dv$ as v increases, increasing the normalization factor of the distribution.

The two straight lines in Figure 3*b* are the limit lines imposed by the selection criterion for this sample, calculated as

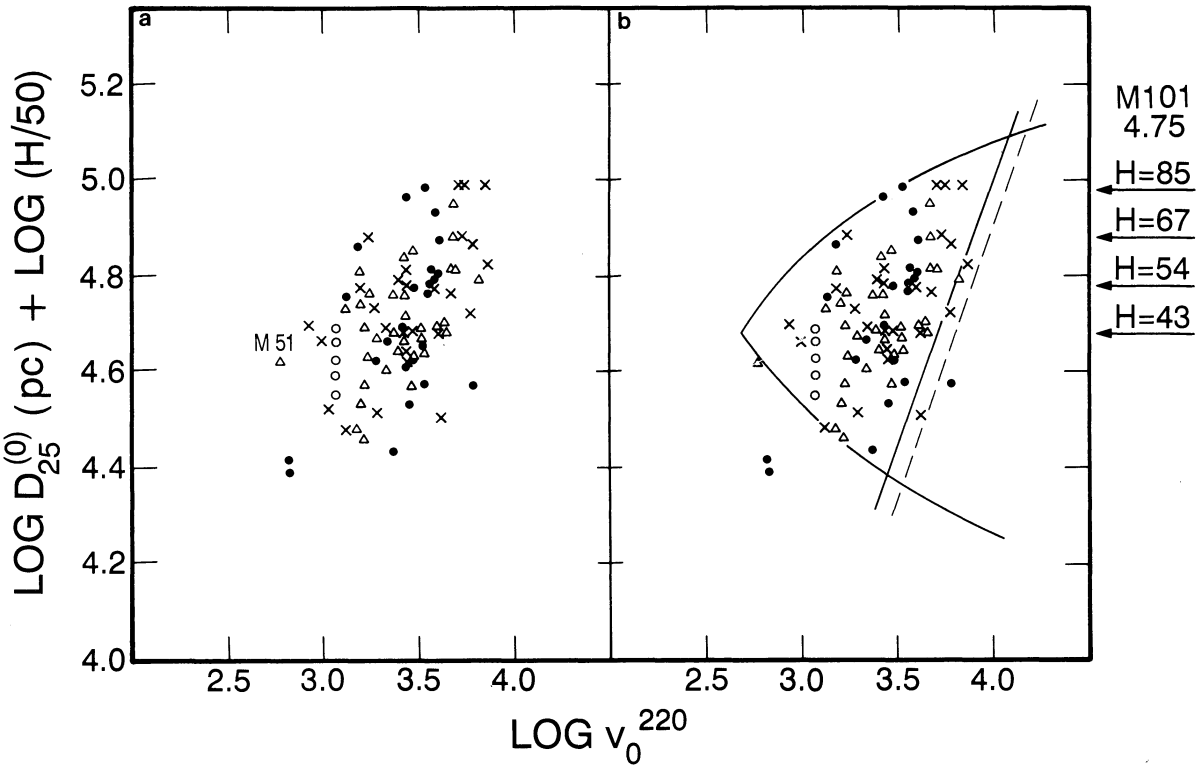

FIG. 3.—(*a*) Calculated linear diameters (pc) based on RC2 angular diameters corrected to face-on and redshift distances based on v_0^{220} redshifts using $H = 50$ km s^{-1} Mpc^{-1} vs. the log of the redshift (v_0^{220}) corrected to the Virgo Cluster frame. Data are from Tables 2–4. Open circles are the four Virgo Cluster spirals in Table 1 plus NGC 4654; crosses are Sc I–I.3, SBc I–I.3 galaxies from Table 2; filled circles are for Sbc I–I.3, SBbc I–I.3 galaxies from Table 3; triangles are for Sbc I–II, SBbc I–II galaxies from Table 4 with 0.03 added to their log D values. (*b*) Same as (*a*) but with the envelope lines that define the loci of one galaxy in the diameter distribution. The straight solid and dashed lines define the selection boundaries caused by the flux limitation at $B = 13$ mag of the Shapley-Ames catalog (see text).

follows. Galaxies that would occupy the area between the upper and lower envelope lines to the right of these limit lines are not contained in the RSA. They are fainter (and therefore smaller in angular size) than the apparent magnitude limit of $B = 13$ in that catalog.

The tight relation between absolute magnitude $M_{B,T}^{0,i}$ (col. [7] of Tables 2–4) and log D_{25} (col. [6] of Tables 2–4) is shown in Figure 4. The absolute magnitudes are based on $B_T^{0,i}$ from the RSA, calculated from the v_0^{220} redshifts in column (3), using $H_0 = 50$. The position of M101 in this diagram is explained later.

The equation of the ridge line in Figure 4 is

$$\log D(\text{pc}) = -0.22 M_{B,T} - 0.15 \qquad (2)$$

for $H_0 = 50$. (Eq. [2] is nearly independent of H_0. It would, of course, be entirely independent if the coefficient on M would be -0.20.)

Imposing the RSA catalog limit of $B = 13$ on the sample in Figure 4 permits calculation of the corresponding absolute magnitude at any redshift (using $H = 50$), from which the corresponding limiting log D value follows from equation (2). In this way the ridge line in Figure 4 is transferred as the solid line into Figure 3*b*; the lower envelope line in Figure 4 is the dashed line in Figure 3*b*, calculated in the same way.

Clearly, the increase in the linear diameters with redshift in Figure 3*a* is due to the progressive incompleteness of the magnitude-limited sample with increasing redshift (i.e., the Malmquist bias). The proof was shown elsewhere (S88a, b) by adding a fainter sample to the equivalent of Figures 3*a* and 3*b*.

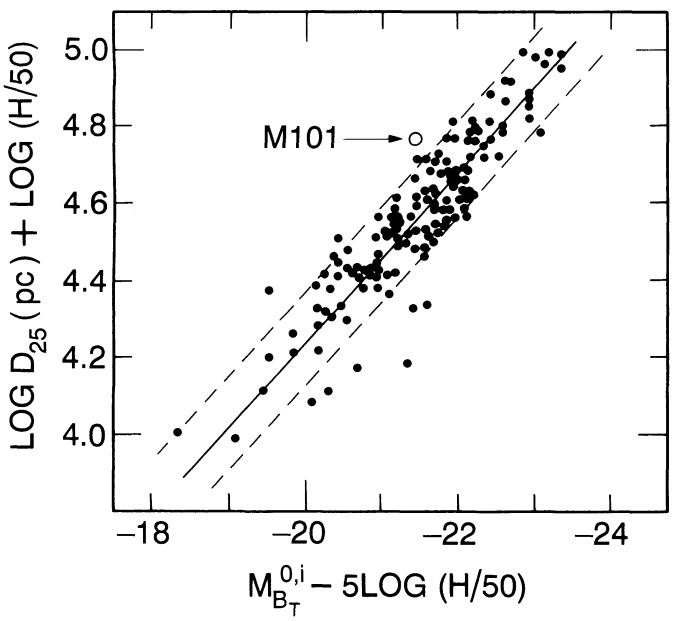

FIG. 4.—Correlation of the absolute magnitudes and linear diameters of the sample galaxies based on RC2 diameters and RSA $B_T^{0,i}$ magnitudes. Data are from Tables 2–4 plus data for Sc II types (data not given in the text) that extend the correlation to fainter and smaller galaxies. The ridge line translates into the solid straight line in Fig. 3*b*. The lower dashed line translates into the dashed line in Fig. 3*b*.

5.2. *The Vertical Position of the Apex in Figure 3b*

The position of the envelope lines in Figure 3*b* is crucial; the vertical position of the apex contains the solution to H by this method.

In S88a we set the apex position by eye using vertical and horizontal shifts of the upper and lower envelope lines relative to the data in the M_B, log v plot. The error of the apex absolute magnitude by this fit was estimated to be ~ 0.2 mag (footnote 9 of S88a). By equation (2) this would translate to an apex uncertainty of ~ 0.04 in log D in Figure 3. A more thorough analysis of the present data is now given by considering the distribution of log D in given redshift intervals in Figure 3*a*.

Figure 5 shows histograms of the linear diameters in four redshift intervals whose boundaries range between $3.1 < v_0^{220} < 3.9$. The data are the same as plotted in Figure 3*a* and are from Tables 2–4. The Malmquist bias is shown by the progressive increase in the position of the arrows as the redshift increases from the top to the bottom panel. The increase of log D with redshift is also seen in Figure 5 which is a different representation than the same data in Figure 3*a*. The arrows are at $\langle \log D \rangle$ values of 4.68, 4.70, 4.76, and 4.83 in Figure 5 for the redshift intervals between log v of 3.1–3.3 to 3.7–3.9, respectively. Figure 3*b* shows that the first of these intervals is bias-free because all the data are contained between the upper and the lower envelope lines. Note that the limit lines intersect the lower envelope curve near log $v_0^{220} = 3.4$ showing where the sample ceases to be distance-limited.

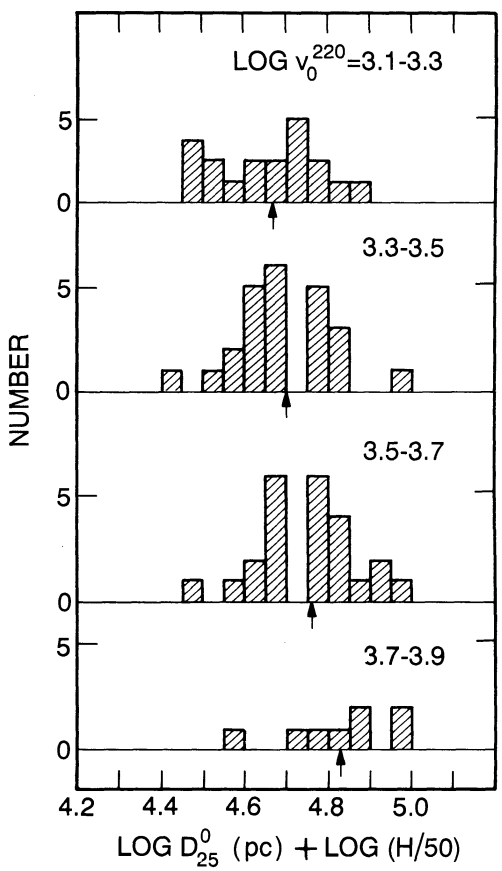

FIG. 5.—Histograms of the distribution of linear diameters in four redshift intervals from the data in Fig. 3. The arrows are the mean values of log D at 4.68, 4.70, 4.76, and 4.83 in the progressive redshift intervals from top to bottom. The increase in $\langle \log D \rangle$ with increasing redshift, shown also in Fig. 3*a* in a different representation, is the Malmquist bias effect.

To test if the observed variation of $\langle \log D \rangle$ with redshift is reasonable and is due to the Malmquist bias, we calculate the bias effect of the incompleteness (Fig. 3*b*) assuming a Gaussian distribution of log D in each redshift interval, progressively truncating the distribution at small log D values by the solid limit line in Figure 3*b*. The resulting mean log D in each redshift interval is then calculated. This procedure, which simply illustrates the classical Malmquist bias *for each distance interval*, is given by

$$\Delta\langle \log D \rangle = \frac{\int_{\Delta(\log D)v}^{+\infty} \operatorname{erf}(\Delta \log D/\sigma) f(D, v)(\Delta \log D) d(\Delta \log D)}{\int_{-\infty}^{+\infty} \operatorname{erf}(\Delta \log D/\sigma) f(D, v) d(\Delta \log D)}, \quad (3)$$

where $\Delta \log D \equiv \log D - \langle \log D \rangle$. The lower limit of the integration in the numerator is the position of the adopted limit line in Figure 3*b*. The parameter $f(D, v)$ is the incompleteness factor calculated from the magnitude incompleteness factor $f(m)$ between $B = 12$ and $B = 13$ in the RSA catalog (Sandage, Tammann, & Yahil 1979, hereafter STY) changed in an obvious way to incompleteness in the angular diameter distribution.

With $f(D, v)$ put equal to 1, the calculated corrections to $\langle \log D \rangle_v$ using the dashed limit line in Figure 3*b* are 0.000, −0.002, −0.016, and −0.06 in the redshift intervals of log v between 3.1–3.3, 3.3–3.5, 3.5–3.7, and 3.7–3.9, respectively. The calculated corrections for the solid line in Figure 3*b* are 0.000, −0.012, −0.038, and −0.120 in the same respective redshift intervals.

The *observed* corrections to $\langle \log D \rangle_v$ in particular redshift intervals are 0.00, −0.02, −0.08, and −0.15 for log v between 3.1–3.3, 3.3–3.5, 3.5–3.7, and 3.7–3.9, respectively, read from the arrow positions in Figure 5, zero-pointed by the arrow position in the lowest redshift interval which is bias free.

These observed corrections, shown by the movement of the arrows in Figure 5, are slightly larger than the two sets of calculated corrections. Consequently a third set of corrections was calculated based on a limit line farther to the left of the two in Figure 3*b* by an amount equal to their separation. This was done to account for the known $f(m)$ *progressive* incompleteness of the RSA catalog between $B = 12$ and $B = 13$ (STY 1979). The need to move leftward from this line is also evident from the data themselves; the points in Figure 3*b* thin out, not forming a sharp boundary close to the solid limit line in the diagram.[2]

The third set of calculated Malmquist corrections is 0.00, −0.012, −0.060, and −0.20 for the same log v redshift intervals of 3.1–3.3, 3.3–3.5, 3.5–3.7, and 3.7–3.9, respectively.[3]

The final adopted Malmquist corrections, when applied to the observed $\langle \log D \rangle$ values (Fig. 5) give the apex position of

[2] The equation of this third limit line (not shown) is

$$\log D = \log v - 3.64, \quad (4)$$

required as the lower integration limit in the numerator of eq. (3). This equation approximates the more exact continuous incompleteness factor $f(m)$ of STY (1979).

[3] The correction calculated from eq. (3) is, of course, most sensitive at large redshifts near the intersection of the upper envelope line and the limit line in Fig. 3*b*. Hence, the calculated correction of −0.20 for the last redshift interval is more uncertain than the other values at lower redshifts.

the envelope lines to be

$$\log D + \log (H/50) = 4.68 \pm 0.02 . \quad (5)$$

This is the same value as found from the bias-free first redshift interval. The quoted error of 0.02 is calculated by applying 0.000, −0.012, −0.060, and −0.20 to the observed $\langle \log D \rangle$ values of 4.68, 4.70, 4.76, and 4.83 in the same redshift intervals and calculating the variance.

5.3. *The Horizontal Position of the Apex in Figure 3b*

The position of the apex along the redshift axis defines the volume in velocity space that must be surveyed before one Sc I galaxy of the M101 type is expected to be found.

As in S88a, b, we have determined this position by sliding a family of template envelope lines of different $\sigma(\log D)$ dispersion values (similar to Fig. 11 of S88a in M, log v space) horizontally until the best fit to the distribution of the data in Figure 3*a* is obtained. The present procedure is more highly constrained than in S88a, b, and therefore the apex position is better determined.

Envelope curves with $\sigma(\log D)$ values ranging from 0.08 to 0.12 were generated by the procedure described in § 5.1. The best fit of the envelope lines in Figure 3*b* is with $\sigma(\log D) = 0.10$, close to the calculated dispersion of $\sigma(\log D) = 0.11$ from the data themselves in Figures 3*a* and 5 in each redshift interval.

All but two data points are accommodated[4] by the fit in Figure 3*b*. The apex is put at log $v = 2.70$. The redshift of $v_0 = 500$ km s^{-1} is close to that of the M101 group itself, showing the internal consistency of the model.

6. THE HUBBLE CONSTANT FROM THE APEX POSITION IN THE log D, log V DIAGRAM

The most probable position of M101 in Figure 3*b* is at the apex of the envelope lines because it is the nearest Sc I galaxy to the Local Group.

From the distance and angular diameter of M101 adopted in § 4.1, the log of the linear diameter is

$$\log D_{25}(\text{M101, pc}) = 4.75 \pm 0.04 . \quad (6)$$

The estimated error is compounded from an assumed ±0.2 mag error in the adopted distance modulus and $a \pm 5\%$ error in the angular diameter of M101.

Combining equations (5) and (6) gives the local value of the Hubble constant as

$$H = 43 \pm 5 \text{ km s}^{-1} \text{ Mpc}^{-1} . \quad (7)$$

The quoted uncertainty is the internal error compounded of the error in the M101 distance, its angular diameter, and the uncertainty of the apex position in Figure 3*b*.

The larger external error is based on the uncertainty inherent in the assumption that M101 is at the apex position. With $\sigma(\log D) = 0.10$ as adopted, a 1 σ deviation of the M101 linear diameter from the apex position would give an apex calibration of $\langle \log D(\text{pc}) \rangle$ either 4.85 or 4.65 instead of 4.75.

Because H from equation (7) is already so low, it is unlikely that the direction of a 1 σ deviation of M101 from the most probable value would be in the direction of making H even smaller. Therefore, we consider the deviation of the M101 diameter from the most probable value only in the direction to make H larger.

A 1 σ deviation in the ordinate of the apex in Figure 3*b* using $\langle \log D \rangle = 4.65$ gives $H = 54$ km s^{-1} Mpc^{-1}, marked along the right-hand border of Figure 3*b*. Such a deviation will occur 34 times out of 100 simulations in a normal distribution, considering only the one direction in the log D deviation that makes H larger.

A 2 σ deviation gives $H = 67$, while if M101 is 3 σ larger than the mean of the field Sc I galaxies, $H = 85$.

The intersection of the 3 σ arrow along the border of Figure 3*b* with the upper envelope line shows that if we require H to be 85 km s^{-1} Mpc^{-1}, M101 must be as large as the largest Sc I galaxies in the volume encompassed by the redshift distance of ~4000 km s^{-1}. Said differently, to reach linear diameters that are so much larger than the mean diameter requires sampling a large enough volume so that we are far enough in the sparse wings of the log D distribution that a 3 σ deviation contains one galaxy; the volume normalization factor must be so large as to meet this condition. Figure 3*b* shows that to require M101 to have such a large linear diameter is unlikely enough to exclude $H = 85$ to at least the 1% level. This indeed is about the correct level based on ~ one galaxy out of a sample of ~100 at this diameter in the diagrams.

The most probable value of H from these data is, then,

$$H = 43 \pm 11 \text{ km s}^{-1} \text{ Mpc}^{-1} , \quad (8)$$

where the external error is based on $\sigma(\log D) = 0.10$.

Equation (8) refers to the expansion property of the field galaxies in Tables 2–4 whose mean redshift is ~3000 km s^{-1}. Previous studies have shown that such a local sample defines the same Hubble diagram and therefore the same Hubble constant as more distant galaxies that define the global frame, to within our ability to measure such velocity deviations from the cosmic flow (Sandage, Tammann, & Hardy 1972; Sandage & Tammann 1975). The Hubble constant does not change systematically outward (S88a, b).

Nevertheless, it is not yet clear how to relate equation (8) to the cosmic Machian frame *precisely*. For example, if the local supercluster is in bulk motion, falling as a unit toward the microwave background (Tammann & Sandage 1985), yet expanding internally at the cosmic rate, then equation (8) will give the cosmic value, H_0. If, however, there are velocity gradients in the expansion field (retardations depending on nonisotropic gravity forces caused by nonisotropic mass concentrations on a scale of order 5000 km s^{-1}) then equation (8) will differ from H_0 at some level (Sandage 1975). But the deviation is expected to be small because Tables 2–4 contain galaxies in all directions of the sky, smoothing out velocity gradients, leaving only any bulk motion.

The maximum effect of bulk motion is less then 400 km s^{-1} (Tammann & Sandage 1985; Jerjen & Tammann 1992) over the mean distance of the present sample at 3000 km s^{-1}. Hence, the largest systematic effect will be of the order of 400/3000 = 13%. Therefore, the largest value of the cosmic expan-

[4] The two galaxies outside the envelope lines in Fig. 3*b* are NGC 3344 and NGC 3486, both from Table 3, at v_0 redshifts of 627 km s^{-1} and 636 km s^{-1}, respectively, from the RSA. These galaxies undoubtedly form a physical pair. They are 5°.5 apart in the sky, which at a distance of 10 Mpc (the approximate redshift distance), is a projected linear separation of 1 Mpc—the size of the Local Group.

Their position at RA = 12^{h}50^m, decl. = +27° is near the direction of the highly perturbed local velocity field due to the "infall" of the Local Group (actually the retarded expansion relative to the Virgo Cluster) in the Virgocentric flow model. The velocity corrections for this perturbation are uncertain, making both the ordinate and the abscissa values in Fig. 3 the most uncertain in the sample.

sion rate by this method remains low at $H_0 = 49$ km s^{-1} Mpc^{-1}. This value is equation (8) multiplied by 1.13.

7. M101 AS THE SOLE CALIBRATOR

The principal criticism of the method is use of only one calibrator, necessitated by the circumstance that M101 is the only Sc I galaxy of known distance. We inquire here into the confidence of its average nature or of the absence of evidence to the contrary.

1. There are suggestions that the largest several H II regions in M101 are atypically large (Sandage & Tammann 1974a, b; Kennicut 1981; Teerikorpi 1985), raising the possibility that such abnormalities, if true, signal other nontypical parameters such as disk length and absolute magnitude. Consider first the H II regions themselves.

A. Although the brightest several H II regions are large in halo dimensions (Sandage & Tammann 1974b), they are normal in core size. Figure 10 of Sandage & Tammann (1974a) shows normal core size. Further, Sandage & Tammann (1974b) show that the H II size calibration (eq. [7] of Sandage & Tammann 1974b), applied to M101 itself, recovers the Cepheid distance of $m - M = 29.3$. Note that M101 itself was not used to make the calibration.

B. The identification of the largest H II regions as belonging to M101 itself is uncertain. NGC 5471, detached from the main body, may be a separate satellite galaxy rather than the largest H II region per se.

C. The halo diameters of the other large H II regions, such as NGC 5462 and NGC 5461, are ill-defined. They form a common envelope of several overlapping associations that may be incorrectly identified as the largest *individual* H II regions.

2. The $B - V$, absolute magnitude correlation for Sc I galaxies discovered by Teerikorpi (1982, Table 2) requires $H = 41$ km s^{-1} Mpc^{-1} from a method using colors of field Sc I galaxies identical to the method used here with angular diameters. If, then, the scale length of M101 is abnormal, so must be its $B - V$ color in such a way to give the same value of H.

3. The strongest suggestion for a possible atypicality is the nearly isolated position of M101 in the luminosity-diameter relation in Figure 4, showing that M101 has marginally low surface brightness. If this is real and due to abnormally large size for its absolute magnitude, the correction to log D to place it on the ridge line in Figure 4 is $\Delta \log D = 0.19$ which would change equations (7) and (8) from $H = 43$ to $H = 66$.

However, M101 in Figure 4 is only marginally abnormal in its position. The mean surface brightness from the $D(25)^{RC2}$, $M^{RSA}_{(B,T)}$ data in Tables 2–4, is $\langle SB \rangle = 22.8$ B arcsec^{-2} with a standard deviation for the total sample of 0.37 mag. The SB of M101 using log $D(25)^{RC2} = 4.75$ and $M(B_T) = -21.41$ is 23.7 B arcsec^{-2}, giving a marginal deviation of 2.4 σ. Using diameters and corrected B^0_T magnitudes from the RC3, described in the next section, gives $\langle SB \rangle = 23.2$ B arcsec^{-2} for the total sample (91 galaxies) with a standard deviation of 0.46 mag. The M101 data with log $D(25)^{RC3} = 4.78$ and $M_{(B,T)} = -21.19$ gives $\langle SB \rangle_{M101} = 24.1$ which differs marginally from the mean by 2.0 σ. Note that if the RSA $B^{0,i}_T$ magnitude of 7.89 rather than 8.19 had been used, the deviation is reduced to 1.3 σ.

8. RELIABILITY OF THE DATA

The analysis to this point depends on angular diameters from the RC2 (de Vaucouleurs et al. 1976) and $B(T)^{0,i}$ magnitudes from the RSA. To determine the sensitivity of the result to the input data, we have redone the analysis using diameters and magnitudes from the Third Reference Catalog (de Vaucouleurs et al. 1991, hereafter RC3).

The precepts for reduction of observed angular diameters and apparent magnitudes to face-on orientation for the effects of inclination differ fundamentally between the RC2 and RC3. In the RC3, the adopted correction model assumes opaque disks for spirals, whereas the RC2 correction, like the RSA, adopted the less extreme Holmberg precepts for disk absorption. Because M101 is nearly face-on, it differs less than the other galaxies in the corrections relative to more inclined galaxies in the sample. Hence, the details of the data differ whether RC2, RC3, and RSA data are used.

Figure 6*a* shows RC2 diameters and RSA magnitudes for the sample in Tables 2–4 in the unbiased distance-limited range of log $v_0^{220} < 3.4$. This diagram shows a subsample of the

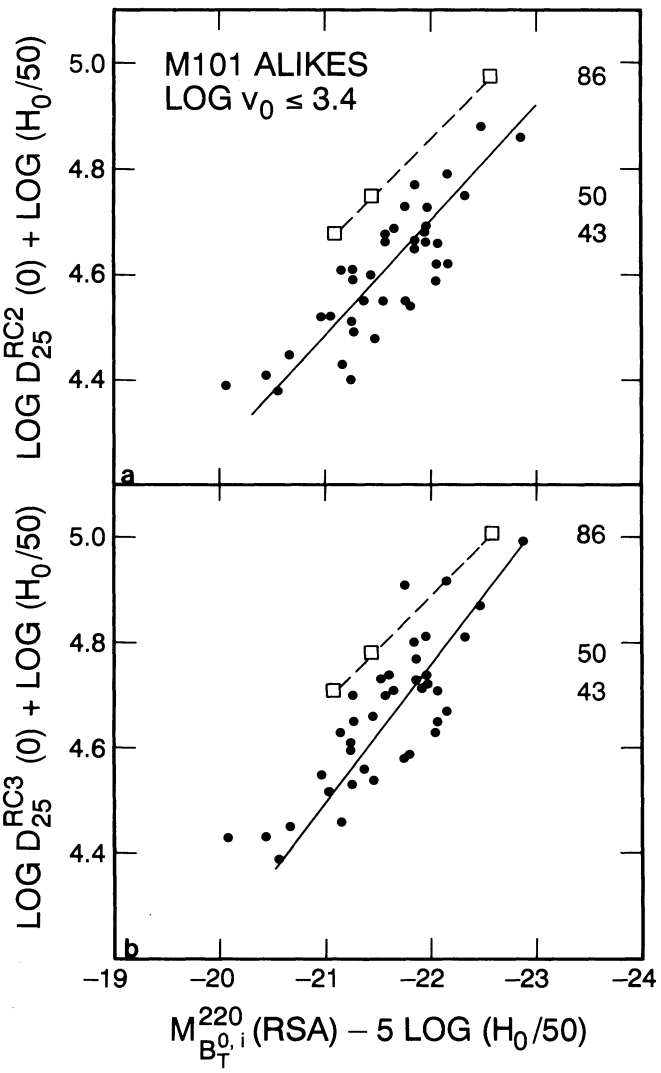

FIG. 6.—(*a*) The correlation of linear diameter and absolute magnitude for the distance limited subsample from Tables 2–4 using RC2 angular diameters and RSA apparent magnitudes corrected for Galactic absorption and inclination effects. The position of M101 for H values of 86, 50, and 43 km s^{-1} Mpc^{-2}, based on (log $D)_{M101} = 4.75$, $M_{(B,T)M101} = -21.41$ are shown. (*b*) Same as (*a*) but using RC3 diameters and RSA magnitudes. The M101 data point is based on log $D_{M101} = 4.78$ and $M_{(B,T)M101} = -21.41$.

complete data set out in Figure 4. The three boxes are for H values of 86, 50, and 43 km s^{-1} Mpc^{-2}. [Note that the M101 values are fixed at log $D(25)^{RC2} = 4.75$, $M^{RSA}_{(B,T)} = -21.41$, but that the field galaxies move in ordinate and abscissa for the different H values.) M101 is still marginally deviant, either by Δ log $D = 0.16$ or $\Delta M = 0.8$ mag, but again only at the $\sim 1.5\,\sigma$ level.

But the point of the method is to note that if $H = 86$, then M101 would again be the largest galaxy in the distance-limited sample defined by log $v_0 < 3.4$. *The conclusion does not change whether M101 is atypical or not in surface brightness.*

Figure 6*b* shows RC3 diameters using RSA magnitudes. Here the deviations of M101 in surface brightness from the rest of the sample is less pronounced than in Figure 6*a*.

Figure 7*a* shows RC3 diameters and RSA magnitudes. Figure 7*b* gives RC3 diameters and RC3 magnitudes, showing (1) M101 is again only marginally atypical in surface brightness, and (2) as before, if $H = 86$, then M101 is the largest Sc I galaxy in the volume contained within log $v_0^{220} < 3.4$.

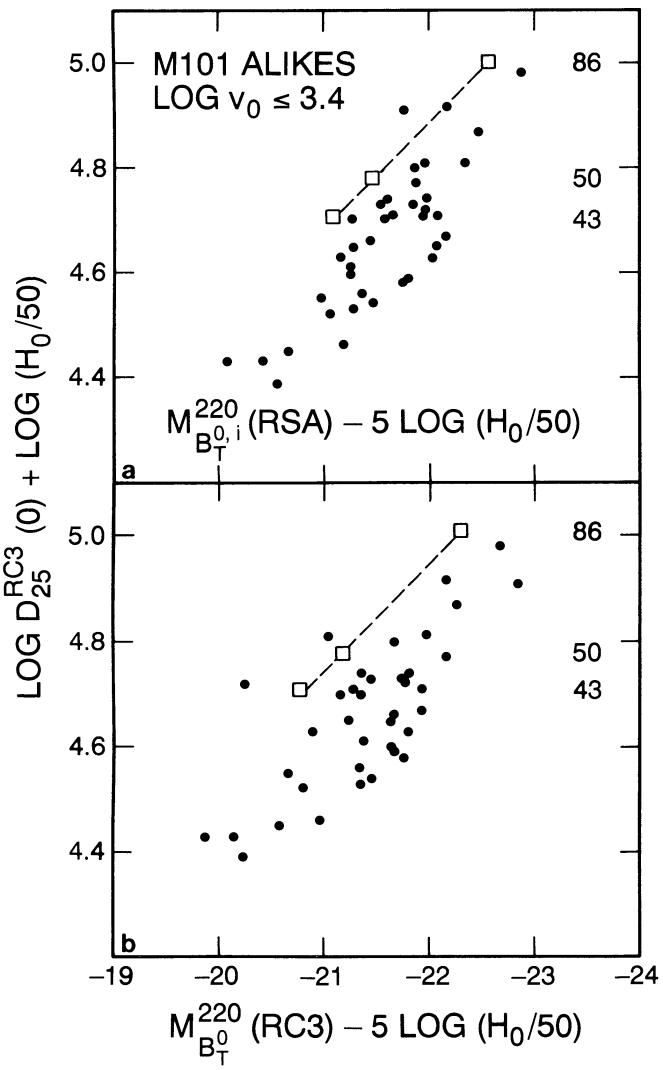

FIG. 7.—(*a*) Same as Fig. 6*b*. (*b*) The data are RC3 diameters and RC3 corrected magnitudes. The M101 data are based on log $D = 4.78$, $M_{(B,T)} = -21.11$.

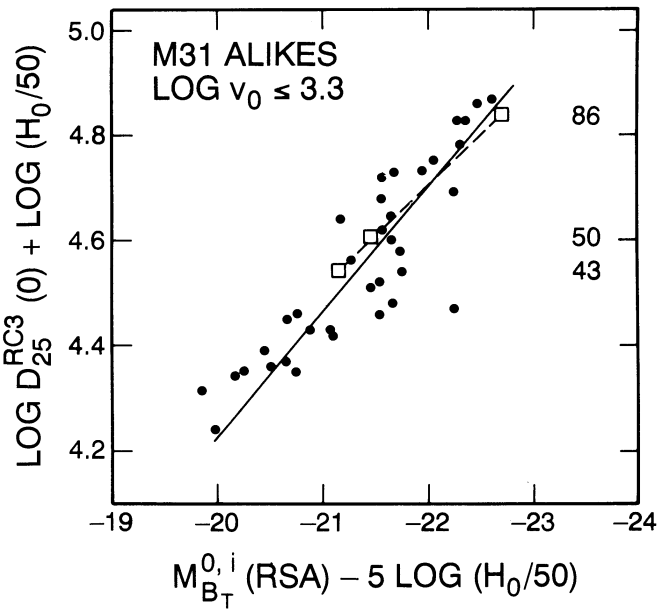

FIG. 8.—The diameter, absolute magnitude diagram for galaxies with the M31 Sb morphology using RC3 diameters and RSA corrected magnitudes. The sample is distance-limited and is therefore free of Malmquist bias. The three boxes show the position of M31 based on $(m - M)_0 = 24.2$ giving $(\log D)_{M31} = 4.62$, $M(B_T^{0,i})_{M31} = -21.49$.

9. THE TEST USING M31

Following van der Kruit (1986), we have applied the method to Sb field galaxies similar in morphology to M31. Details of the sample and of individual data are given elsewhere (Sandage 1993). The result, similar to Figures 6 and 7, is shown in Figure 8. The sample is distance limited at log $v_0 = 3.3$. Data in this unbiased region are shown in Figure 8 using RC3 diameters and RSA magnitudes. The data for M31, based on $(m - M)_0 = 24.2$, are log $D(\mathrm{pc})^{RC3} = 4.61$ and $M(B_T)^{RSA} = -21.49$.

Again, the conclusion is that if $H = 86$ km s^{-1} Mpc^{-1} M31 would be as large and as bright as the largest and brightest Sb I galaxy within log $v_0 = 3.3$. At the most probable value of the mean $\langle \log D \rangle$ for the sample, calibrated by M31, $H = 47 \pm 10$ km s^{-1} Mpc^{-1} using Sb and Sbc galaxies alone (Sandage 1993), based on the equivalent to Figure 3 but for Sb galaxies.

The result shows that the method here of using M101 alone cannot be faulted by claiming M101 to be abnormal unless, of course, M31 is equally abnormally large.

10. CONCLUSIONS AND SUMMARY

Eight methods set out in the introduction have been discussed using data from the cited literature as leading to the long distance scale with H_0 near 50 km s^{-1} Mpc^{-1}; two other methods using planetary nebulae and surface brightness fluctuations support the short scale that requires H_0 to be near 85. A ninth method that requires the long distance scale with H(local) = 43 km s^{-1} Mpc^{-1} is set out here using linear sizes of Sc spiral galaxies in the field.

If H_0 would be as high as 86, then one of two unlikely propositions must be true. (1) Our adopted distance to M101 of 7.24 Mpc ($m - M = 29.3$) must be too large by a factor of 2 making $m - M = 27.8$ for it, or (2) M101 is in fact the largest

Sc I galaxy in the local neighborhood. In a normal distribution of log D diameters, this is unlikely at the 1% level.

The first possibility is out of the question, given our inability to find Cepheids in an exhaustive search of M101 (Sandage & Tammann 1974b) on a long series of 200 inch plates that were as deeply exposed as were the plates for NGC 2403 with $m - M = 27.6$. Cepheids were found in NGC 2403 in great numbers (Tammann & Sandage 1968).

The second possibility that M101 is 3 σ larger than the mean diameter of the Sc I distribution cannot be ruled out except on the probability argument just given. Yet someone must be living close to the largest known Sc I galaxy somewhere in the universe (George Carlson's comment). That it is not us is supported by the analysis of M31 relative to Sb look-alikes in the field (Fig. 8). Our conclusion here is the same reached by van der Kruit (1986) using M31 and our Galaxy as standards, that $H_0 < 50$ km s^{-1} Mpc^{-1}.

It is a pleasure to thank L. Bottinelli for her perceptive, helpful, and kind refereeing of an early draft of the paper and for her suggestions for the arguments concerning the normalcy of M101. Helpful comments on these and additional points were also made by P. Teerikorpi to whom we are also grateful.

REFERENCES

Aaronson, M., et al. 1982, ApJS, 50, 241
Bartel, N. 1989, in Supernova Shells and Their Birth Events, ed. W. Kundt (Berlin: Springer-Verlag), 206
Binggeli, B., Sandage, A., & Tammann, G. A. 1985, AJ, 90, 1681
Birkinshaw, M., Hughes, J. P., & Arnaud, K. A. 1991, ApJ, 379, 466
Boroson, T. 1981, ApJS, 46, 177
Boroson, T. A., Strom, K. M., & Strom, S. E. 1983, ApJ, 274, 39
Bottinelli, L., Gouguenheim, L., Paturel, G., & Teerikorpi, P. 1991, A&A, 252, 550
Branch, D., Falk, S. W., McCall, M. L., Rubski, P., Uomoto, A. K., & Wells, B. J. 1981, ApJ, 244, 780
Cook, K. H., Aaronson, M., & Illingworth, G. 1986, ApJ, 301, L45
de Vaucouleurs, G., de Vaucouleurs, A., & Corwin, H. G. 1976, Second Reference Catalog of Bright Galaxies (Austin: Univ. of Texas Press) (RC2)
de Vaucouleurs, G., de Vaucouleurs, A., Corwin, H., Buta, R. J. Paturel, G., & Fouqué, P. 1991, Third Reference Catalog of Bright Galaxies (Berlin: Springer-Verlag) (RC3)
Disney, M. J. 1976, Nature, 263, 573
Dressler, A., Faber, S. M., Burstein, D., Davies, R. L., Lynden-Bell, D., Terlevich, R. J., & Wegner, G. W. 1987, ApJ, 313, L37
Fouqué, P., Bottinelli, L., Gougenheim, L., & Paturel, G. 1990, ApJ, 349, 1 (FBGP)
Freeman, K. C. 1970, ApJ, 160, 811
———. 1978, in IAU Symp. 77, Structure & Properties of Nearby Galaxies, ed. E. M. Berkhuysen & R. Wielebinski (Dordrecht: Reidel), 3
———. 1979, in Photometry, Kinematics, Dynamics of Nearby Galaxies, ed. D. S. Evans (Austin: Univ. Texas), 85
Fukugita, M., & Hogan, C. J. 1990, Nature, 347, 120
———. 1991, ApJ, 368, L11 (FH)
Harris, W. E. 1988, in The Extragalactic Distance Scale, ed. S. van den Bergh & C. J. Pritchet (ASP Conf. Ser., 4), 231
Hoflich, P., Khokhlov, A., & Muller, E. 1991, A&A, 248, L7
Holmberg, E. 1950, Medd. Lunds. Obs., 128
———. 1958, Medd. Lunds. Obs., 136
Hubble, E. 1926, ApJ, 64, 321
———. 1936, ApJ, 84, 158
Hubble, E., & Humanson, M. L. 1931, ApJ, 74, 43
Huchtmeier, W. K., & Richter, O.-G. 1986, A&AS, 63, 323
Humason, M. L., Mayall, N. U., & Sandage, A. 1956, AJ, 61, 97
Jacoby, G. H. 1989, ApJ, 339, 39
Jacoby, G. H., Ciardullo, R., & Ford, H. C. 1990, ApJ, 356, 332
Jacoby, G. H., Ciardullo, R., Ford, H. C., & Booth, J. 1989, ApJ, 344, 704
Jerjen, H., & Tammann, G. A. 1992, preprint
Kennicutt, R. C. 1981, ApJ, 247, 9
Kent, S. M. 1985, ApJS, 59, 115
Knapen, J. H., & van der Kruit, P. C. 1991, A&A, 248, 57
Kormendy, J. 1977, ApJ, 217, 406
Kraan-Korteweg, R. C. 1986, A&AS, 66, 255
Kraan-Korteweg, R. C., Cameron, L. M., & Tammann, G. A. 1988, ApJ, 331, 620 (KKCT)
Kraan-Korteweg, R. C., & Tammann, G. A. 1979, Astron. Nach., 300, 181
Lahav, O., Lilje, P. B., Primack, J. R., & Rees, M. J. 1991, MNRAS, 251, 128
Leibundgut, B., & Tammann, G. A. 1990, A&A, 230, 81
Pierce, M. J., McClure, R. H., & Racine, R. 1992, ApJ, 393, 523
Pierce, M., & Tully, R. B. 1988, ApJ, 330, 579
Press, W. H., Rybicki, G. B., & Hewitt, J. N. 1992, ApJ, 385, 416
Pritchet, C. J., & van den Bergh, S. 1987, ApJ, 318, 507
Rhee, G. 1991, Nature, 350, 211
Sandage, A. 1972, ApJ, 178, 25
———. 1975, ApJ, 202, 563
———. 1988a, ApJ, 331, 583 (S88a)
———. 1988b, ApJ, 331, 605 (S88b)
———. 1990, in Clusters of Galaxies, ed. W. R. Oegerle, M. J., Fitchett, & L. Danly (Cambridge: Cambridge University Press), 201
———. 1993, ApJ submitted
Sandage, A., & Bedke, J. 1993, Carnegie Atlas of Bright Galaxies (Carnegie Institution of Washington: Washington, D.C.)
Sandage, A., Binggeli, B., & Tammann, G. A. 1985, AJ, 90, 395
Sandage, A., & Tammann, G. A. 1974a, ApJ, 190, 525
———. 1974b, ApJ, 194, 223
———. 1975, ApJ, 196, 313
———. 1976, ApJ, 210, 7 (Paper VII)
———. 1982, ApJ, 256, 339 (Paper VIII)
———. 1987, A Revised Shapley-Ames Catalog (2d ed.; Washington DC: Carnegie Institution of Washington) (RSA2)
———. 1988, ApJ, 328, 1
———. 1990, ApJ, 365, 1 (ST90)
Sandage, A., Tammann, G. A., & Hardy, E. 1972, ApJ, 172, 253
Sandage, A., Tammann, G. A., & Yahil, A. 1979, ApJ, 232, 352 (STY)
Sandage, A., Saha, A., Tammann, G. A., Panagia, N., & Macchetto, D. 1993, ApJ, in press
Schechter, P. L. 1980, AJ, 85, 801
Segal, I. 1982, ApJ, 252, 37
Shanks, T., Tanvir, N. R., Major, J. V., Doel, A. P., Dunlop, C. N., & Meyers, R. M. 1992, MNRAS, 256, P29
Silk, J. 1974, ApJ, 193, 525
———. 1977, A&A, 59, 53
Tammann, G. A. 1988, in The Extragalactic Distance Scale, ed. S. van den Bergh & C. J. Pritchet (ASP Conf. Ser., 4), 282
———. 1992, Phys. Scripta, in press
Tammann, G. A. & Leibundgut, B. 1990, A&A, 236, 9
Tammann, G. A., & Sandage, A. 1968, ApJ, 151, 825
———. 1985, ApJ, 294, 81
Teerikorpi, P. 1982, A&A, 109, 314
———. 1985, A&A, 143, 469
Teerikorpi, P., Bottinelli, L., Gougenheim, L., & Paturel, G. 1992, A&A, 260, 17
Tonry, J. L., Ajhar, E. A., & Luppino, G. A. 1989, ApJ, 346, L57
Tonry, J. L., & Davis, M. 1981, ApJ, 246, 680
Tonry, J. L., & Schneider, D. 1988, AJ, 96, 807
Tully, B. 1988, Nature, 334, 209
Tully, R. B. & Shaya, E. J. 1984, ApJ, 281, 31
van der Kruit, P. 1986, A&A, 157, 230
———. 1987, A&A, 173, 59